[This is a post-referring version, Accepted in the International Journal of Applied Earth Observation and Geoinformation]
Link to the published (open access) version: https://doi.org/10.1016/j.jag.2019.101992

Realistic and simplified models of plant and leaf area indices for a seasonally dry tropical forest

Rodrigo de Queiroga Miranda[1*], Rodolfo Luiz Bezerra Nóbrega[2,3], Magna Soelma Beserra de Moura[2,4], Raghavan Srinivasan[5], Josiclêda Domiciano Galvíncio[1]

[1]*Laboratório de Sensoriamento Remoto e Geoprocessamento, Universidade Federal de Pernambuco, Recife, Pernambuco, Brazil, 50670901*

[2]*Department of Geography and Environmental Science, University of Reading, RG6 6AH Reading, UK*

[3]*Department of Life Sciences, Imperial College London, SL5 7PY Ascot, UK*

[4]*Brazilian Agricultural Research Corporation – Embrapa Semi-arid, Petrolina, Pernambuco, Brazil, 56302970*

[5]*Spatial Sciences Laboratory, Texas A&M University, College Station, TX 77845, USA*

[*]*Corresponding author*

R. Q. Miranda
Tel.: +55(81)2126-7375; E-mail: rodrigo.qmiranda@gmail.com; ORCID: 0000-0002-5464-2397

R. L. B. Nóbrega, r.nobrega@imperial.ac.uk
ORCID: 0000-0002-9858-8222

J. D. Galvíncio
ORCID: 0000-0001-7367-6587

M. S. B. Moura
ORCID: 0000-0002-2844-1399

R. Srinivasan
ORCID: 0000-0001-8375-6038

[This is a post-referring version, Accepted in the International Journal of Applied Earth Observation and Geoinformation]
Link to the published (open access) version: https://doi.org/10.1016/j.jag.2019.101992

Abstract

Leaf Area Index (LAI) models that consider all phenological stages have not been developed for the Caatinga, the largest seasonally dry tropical forest in South America. LAI models that are currently used show moderate to high covariance when compared to *in situ* data, but they often lack accuracy in the whole spectra of possible values and do not consider the impact that the stems and branches have over LAI estimates, which is of great influence in the Caatinga. In this study, we develop and assess PAI (Plant Area Index) and LAI models by using ground-based measurements and satellite (Landsat) data. The objective of this study was to create and test new empirical models using a multi-year and multi-source of reflectance data. The study was based on measurements of photosynthetic photon flux density (PPFD) from above and below the canopy during the periods of 2011–2012 and 2016–2018. Through iterative processing, we obtained more than a million candidate models for estimating PAI and LAI. To clean up the small discrepancies in the extremes of each interpolated series, we smoothed out the dataset by fitting a logarithmic equation with the PAI data and the inverse contribution of WAI (Wood Area Index) to PAI, that is the portion of PAI that is actually LAI (LAI_C). LAI_C can be calculated as follows: $LAI_C = 1 - (WAI/PAI)$). We subtracted the WAI values from the PAI to develop our *in situ* LAI dataset that was used for further analysis. Our *in situ* dataset was also used as a reference to compare our models with four other models used for the Caatinga, as well as the MODIS-derived LAI products (MCD15A3H/A2H). Our main findings were as follows: (*i*) Six models use NDVI (Normalized Difference Vegetation Index), SAVI (Soil-Adjusted Vegetation Index) and EVI (Enhanced Vegetation Index) as input, and performed well, with r^2 ranging from 0.77 to 0.79 (PAI) and 0.76 to 0.81 (LAI), and RMSE with a minimum of 0.41 m^2 m^{-2} (PAI) and 0.40 m^2 m^{-2} (LAI). The SAVI models showed values 20% and 32% (PAI), and 21% and 15% (LAI), smaller than those found for the models that use EVI and NDVI, respectively; (*ii*) the other models (ten) use only two bands, and in contrast to the first six models, these new models may abstract other physical processes and components, such as leaves etiolation and increasing protochlorophyll. The developed models used the near-infrared band, and they varied only in relation to the inclusion of the red, green, and blue bands. (*iii*) All previously published models and MODIS-LAI underperformed against our calibrated models. Our study was able to provide several PAI and LAI models that realistically represent the phenology of the Caatinga.

Keywords: Caatinga, Landsat, phenology, semi-arid, Woody Area Index, Leaf Area Index.

1. Introduction

The Leaf Area Index (LAI) is a widely adopted parameter in environmental sciences studies. It represents the one-sided area of leaves that covers a specific surface area (Fotis et al., 2018;

Knote et al., 2009; Mu et al., 2007; Rodriguez et al., 2009) and is one of the main parameters of both global and regional biosphere models (Arnold et al., 1998; Bieger et al., 2017). LAI is used to scale up from leaf to vegetation photosynthesis and transpiration, energy balance of terrestrial surfaces, and many climatological and hydrological attributes such as atmospheric aerosols, water infiltration, and biogeochemical processes (Bonan, 1995).

There are two main approaches used to estimate LAI: (*i*) direct methods, in which the total leaf canopy is obtained by the summation of direct measurement of all individual leaf areas – this is usually a destructive method because it requires the removal of all leaves and, therefore, is not viable at large scales; and (*ii*) indirect methods, which may require active or passive sensors to measure parameters that are highly correlated with LAI, such as light extinction coefficient (Jonckheere et al., 2004); or use the litterfall trap method, which is suitable for estimating LAI of deciduous plants (Almeida et al., 2019). Active sensors do not depend on solar radiation as they emit their own electromagnetic signals and capture those reflected, whereas passive sensors depend on solar radiation and are based on estimating the extent to which a given amount of leaf area will reduce radiation transmitted through a stratified arrangement of leaf elements within a canopy (Zheng and Moskal, 2009). This estimation can be determined using a radiative transfer model such as the PROSPECT and SAIL models (Jacquemoud et al., 2009; Jacquemoud and Baret, 1990; Knyazikhin et al., 1998; Verhoef, 1985, 1984) or abstracted by coefficients of an empirical model (Bastiaanssen, 1998; Galvíncio et al., 2013; Machado, 2014).

Radiative transfer models are highly accurate, but require specific inputs, such as pigment concentration, cell diameter, and water content (Jacquemoud et al., 2009; Jacquemoud and Baret, 1990). These parameters can only be obtained with extensive fieldwork, while empirical models are purely statistical fast retrieval algorithms (Zheng and Moskal, 2009). To estimate LAI, the empirical models are mainly composed of regressions that relate LAI values

to simple spectral responses and greenness indices (Almeida et al., 2019; Galvíncio et al., 2013; Machado, 2014), such as the Soil Adjusted Vegetation Index ($SAVI$) and Normalized Difference Vegetation Index ($NDVI$) (Bastiaanssen, 1998; Galvíncio et al., 2013). For LAI estimations at a regional scale, empirical models are generally reliable (Knote et al., 2009). However, in Brazil, more specifically in the seasonally dry tropical forest (SDTF) in the semi-arid region, known as the Caatinga, models that are currently used have not been developed using both intra- and inter-annual field measurements.

The Caatinga is the largest continuous SDTF in the Americas, with an open and mostly semi-arid landscape, as seen in many inter-plateau depressions (Ab'Saber, 1974; Silva et al., 2017). The Caatinga covers an area of approximately 900,000 km^2 (Silva et al., 2017), and exhibits at least 13 different physiognomies ranging from woodlands to sparsely distributed thorny shrubs (Silva et al., 2017). Its climate is characterized by high temperatures and low rainfall rates with high intra- and inter-annual variability both in space and time. The rainfall is normally concentrated over 2–4 months of the year, with the possibility of over 25% of the annual precipitation occurring in a single rainfall event (Miranda et al., 2018). The main landscape units that can be found in the Caatinga are canyons, ravines, mountains, sandy, and clayey plateaus (Leal et al., 2007). Their complex soil mosaics are commonly formed by four dominant soil orders (Latosols, Lithosols, Argisols, and Luvisols) (Menezes et al., 2012). The Caatinga holds over 3,150 species of 930 genera and 152 families of flowering plants (Silva et al., 2017). These plants have unique adaptations to endure conditions of spatiotemporally irregular water availability and extended droughts: approximately 85% of the Caatinga species lose all their leaves during the dry season (Leal et al., 2003; Silva et al., 2017). Thus, methods that attempt to measure the LAI by directly relating it to the intercepted radiation do not reflect only the area of the leaves, but also the surface of the woody area, which is mainly comprised of stems and branches (Cunha et al., 2019). The influence that stems and branches have over

the LAI estimates can be addressed by computing the LAI as the difference between Plant Area Index (PAI) and the Woody Area Index (WAI) (Kalacska et al., 2005).

Current model estimates of LAI in the Caatinga show moderate to high covariance when compared to *in situ* data (r^2 = 0.60–0.93), but they might lack accuracy in the entire spectra of possible values because they are often developed using observations that do not cover complete intra-annual LAI variations due to phenology (e.g., Almeida et al., 2019; Galvíncio et al., 2013; Machado, 2014). In addition, most of these models applied to the Caatinga have not entirely considered the influence of the continuous variation of WAI, which is highly significant in the Caatinga as over 85% of plant's above-ground biomass is composed of stems and branches (Silva and Sampaio, 2008). The oversight of this uniqueness of SDTFs, such as the Caatinga, is likely to cause methodological drawbacks in estimating LAI. By not considering every all phenological stage, the intra-annual LAI changes may be reduced, and PAI can be wrongly addressed as LAI. As a consequence, models may provide unrealistic values for some periods of the year, especially in the dry season.

In this study, we aimed to create and test new empirical models using a multi-year and multi-source set of reflectance data. We rely on the premise that by providing multiple reflectance data combinations as input and that by accounting for the WAI component of the PAI we will be able to provide models that are more accurate and better adjusted to the Caatinga. Our objectives were to evaluate the efficiency of new LAI models derived from Landsat reflectance using fitted regressions and field measurements from a typical Caatinga formation area in Brazil, and to test new empirical approaches using previously published models currently used for the Caatinga.

Study area

Data were collected in an area of shrubby hyperxerophytic Caatinga forest area (Fig. 1) (Kiill, 2017), located at the Embrapa Tropical Semiarid Research Station in the state of Pernambuco, Brazil (9°2'33"S, 40°19'16"W; at 350 m a.s.l.). The vegetation in this area consists of shrubs, trees, herbaceous plants, and Cactaceae. The canopy average height is 4.5 m. The plant phenological stages in the Caatinga are usually four: foliar development, maturity, senescence, and dormancy (Rankine et al., 2017), and this cycle follows the rainfall patterns closely (Silva et al., 2017). Most species in the Caatinga are deciduous, and respond quickly to slight changes in soil water availability, breaking the dormancy of wood growth; and that allows the plants to sprout most of their leaves in only a few days in the beginning of the rainy season (Machado et al., 1997). The dominant plant species (approximately 90% of the total relative dominance) in our study area were *Commiphora leptophloeos*, *Schinopsis brasiliensis*, *Mimosa tenuiflora*, *Cenostigma microphyllum*, *Sapium glandulosum*, *Cnidosculus quercifolius*, *Handroanthus spongiosus*, *Manihot pseudoglaziovii*, *Croton conduplicatus*, and *Jatropha mollissima* (Kiill, 2017). Although the Cactaceae (*Pilosocereus gounellei* and *Pilosocereus pachycladus)* have a fairly constant vegetative phenology throughout the year, these plants have a relative dominance of less than 5% and an insignificant production of leaves; therefore they were not considered in our LAI estimates. The climate is dry semi-arid (Alvares et al., 2013), with the rainy season between January and April and an average annual temperature of 26°C. Although the average historical annual rainfall is approximately 500 mm, the average rainfall was less than 300 mm during our study period, which is the most severe drought in this region's recorded history. These conditions were particularly interesting for our study, allowing a precise assessment of the WAI influence on the total PAI.

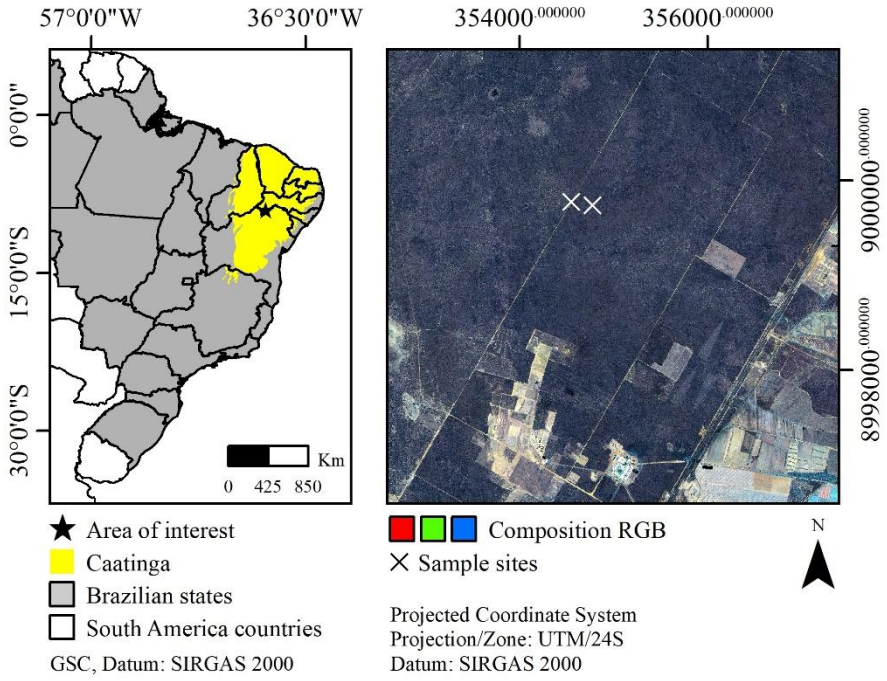

Figure 1. Location of the seasonally dry tropical forest experimental area at the Embrapa Semiarid Research Station in the state of Pernambuco (Brazil).

2. Methodology

Field measurements

LAI was derived from field measurements of photosynthetic photon flux density (PPFD) taken from above and below the canopy using two different non-destructive methods. The measurements were conducted throughout the year in order to cover all plant phenological stages and covered five years: 2011–2012 and 2016–2018. The first method measured PPFD using three quantum sensors (one LI-190SA sensor to measure the above-canopy PPFD, and two LI-191 sensors for the below-canopy data) installed in a 16-m meteorological tower in the study area. All sensors were connected to a data acquisition system (CR1000, Campbell Scientific Inc.), which was programmed to compute averages of 30-s measurements taken at 30-min intervals from January 2011 to December 2012. In order to maximize the quality of our measurements, we filtered all data, considering only the average of the measurements between

10 a.m. and 2 p.m. each day (GMT -3), when the zenith angle is close to zero. The second measurement approach was applied on a weekly basis (68.97% of the entire dataset) from January 2016 to November 2018, with the following exceptions: 19.54% (≥ 8 days of interval between measurements – DBM), 8.05% (≥ 14 DBM) and 3.44% (≥ 21 DBM). The dataset consisted of LAI estimates based on the transmission of light through the canopy at various angles by using an AccuPAR ceptometer (AccuPAR® LP-80, Decagon Devices). The AccuPAR has a linear ceptometer with 80 sensors, capable of measuring PPFD at the photosynthetically active radiation (PAR) range (400–700 nm wavelength) from 0 to 2500 μmol m^{-2}. The above-canopy PPFD and solar zenith angle measurements were obtained in a nearby (about 10 m away) clear area, and the below-canopy PPFD was acquired by holding the AccuPAR beneath the canopy at approximately 0.4 m above ground. The dataset from this approach was linearly interpolated to produce the daily data required to match the satellite overpass times. We used the data collected to predict scattered and transmitted PPFD, as well as to predict light extinction, as proposed by Norman (1979).

[This is a post-referring version, Accepted in the International Journal of Applied Earth Observation and Geoinformation]
Link to the published (open access) version: https://doi.org/10.1016/j.jag.2019.101992

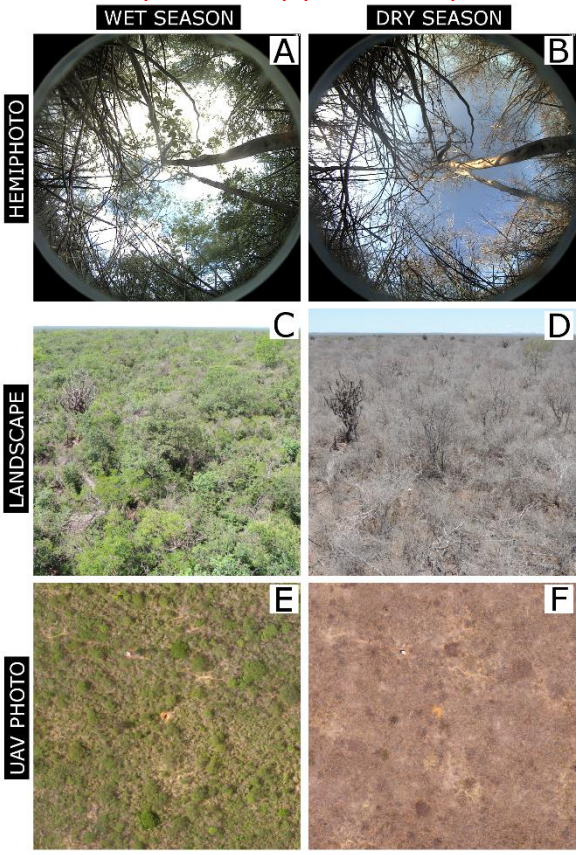

Figure 2. Contrast in the Caatinga between its wet (A, C and E) and dry (B, D and F) conditions. A–B are hemispheric photos taken from below the vegetation in 12/18/2018 and 9/27/2018 respectively; C–D are landscape photos taken horizontally in 2/5/2016 and 10/20/2017 at the height of 14 m; E–F are orthophotos taken by drone (unmanned aerial vehicle) at 80 m height in 02/16/2018 and 10/20/2017, respectively.

Plant Area Index (PAI) partitioning

In our study, we defined PAI as the sum of WAI and LAI (Magalhães et al., 2018), and the WAI as the contribution of woody material such as stems, branches, and trunks to the light interception of PAI. In order to carry out this partition of our data, we first took the minimum LAI (LAI_{MIN}) value of each year as the WAI, which was verified by visual evaluation of hemispheric photos from a phenological monitoring database (Fig. 2); then we fixed this value from the day of the LAI_{MIN} to the first subsequent day with rainfall over 2.5 mm. Based on

field observations, we assumed that low-precipitation ($\leq$ 2.5 mm d^{-1}) events did not cause any significant phenological change in the ecosystem. The WAI was assumed to change between sequential dry seasons gradually; we gap-filled the WAI dataset with a linear interpolation between the fixed-value periods of each year. To avoid small discrepancies in the extremes of each interpolated series, we smoothed the dataset by fitting a logarithmic equation (Eq. 1) with the PAI data and the inverse contribution of WAI to PAI, which is the percentage of PAI that is actually LAI (here called LAI_C). LAI_C was calculated as follows: $LAI_C = 1 - (WAI/PAI)$. The WAI values were subtracted from the PAI to develop our *in situ* LAI dataset, which is used for further analysis.

$$WAI = \{1 - [\ln(PAI) \times 0.5]\} \times PAI \quad (1)$$

Landsat data processing

We selected the Landsat Surface Reflectance Level-2 products for the entire study period (total of 110 candidate images). These products are designed to provide atmospherically and geometrically corrected reflectance data with 30-m resolution for every 16 days. These data are generated using the auxiliary climate data from MODIS (e.g., water vapor, ozone, geopotential height, and aerosol optical thickness) and two different algorithms: 1) the Second Simulation of a Satellite Signal in the Solar Spectrum (6S) algorithm to the data derived from Landsat 5 Thematic Mapper (TM) and Landsat 7 Enhanced Thematic Mapper Plus (ETM+) images; and 2) a unique radiative transfer model to the Landsat 8 Operational Land Imager (OLI) data. The data were extracted from two sample sites (Fig. 1), and all clear pixels were filtered using the respective Quality Band (QA band) of each product (L5–7 = 66, and L8 = 322), resulting in a 70-record dataset. The dataset was then submitted to an iterative model-

[This is a post-referring version, Accepted in the International Journal of Applied Earth Observation and Geoinformation]
Link to the published (open access) version: https://doi.org/10.1016/j.jag.2019.101992

227 fitting approach to create new PAI and LAI models. The Landsat Collection 2 Level-2 products
228 include reflectance values derived from three sensors (TM/Landsat 5, ETM+/Landsat 7, and
229 OLI/Landsat 8) with 30-m spatial resolution. The different bands were matched to create an
230 equivalent dataset of reflectance across all sensors (Table 1). These products are freely
231 available through the LSDS Science Research and Development (LSRD) database of the U.S.
232 Geological Survey (https://espa.cr.usgs.gov/).
233

OLI/Landsat 8 (nm)	ETM+/Landsat 7 and TM/Landsat 5 (nm)	Equivalent bands for this study (nm)
-	$\rho_1^{ETM+/TM}$= 450–520	$\rho_1 = [\rho_2^{OLI}, \rho_1^{ETM+/TM}]$
ρ_2^{OLI}= 452–512	$\rho_2^{ETM+/TM}$= 520–600	$\rho_2 = [\rho_3^{OLI}, \rho_2^{ETM+/TM}]$
ρ_3^{OLI}= 533–590	$\rho_3^{ETM+/TM}$= 630–690	$\rho_3 = [\rho_4^{OLI}, \rho_3^{ETM+/TM}]$
ρ_4^{OLI}= 636–673	$\rho_4^{ETM+/TM}$= 770–900	$\rho_4 = [\rho_5^{OLI}, \rho_4^{ETM+/TM}]$
ρ_5^{OLI}= 851–879	$\rho_5^{ETM+/TM}$= 1,550–1,750	$\rho_5 = [\rho_6^{OLI}, \rho_5^{ETM+/TM}]$
ρ_6^{OLI}= 1,566–1,651	-	-
ρ_7^{OLI}= 2,107–2,294	$\rho_7^{ETM+/TM}$= 2,090–2,350	$\rho_7 = [\rho_7^{OLI}, \rho_7^{ETM+/TM}]$

234 Table 1 - Equivalence table of the bands of the sensors TM/Landsat 5, ETM+/Landsat 7 and
235 OLI/Landsat 8.

236 ***Model calibrations***

237 We developed PAI and LAI models based on the combinations of bands (ρ_1 to ρ_7); vegetation
238 indices ($NDVI$, $SAVI$ and EVI; Eqs. 2 to 4); transformation functions, i.e., x, $1/x$, $\ln(x)$,
239 $\log_{10}(x)$, $\sqrt{x}$, x^2, e^x; and basic mathematical operations. These models were obtained by using
240 an exhaustive training iteration process (> 10^6 iterations) that selected the best results based on
241 the highest coefficient of determination (r^2) with the lowest Root Mean Square Error (RMSE).
242 We used the Percent Bias (PBIAS) and the concordance correlation coefficient (ρ_c) as auxiliary
243 performance indices. In our regression analysis, we used linear, logarithmic, exponential, and
244 power functions to fit the observed data. We obtained $NDVI$, $SAVI$, and Enhanced Vegetation
245 Index (EVI) using Eqs. 2 to 4, where $C1$ (6) and $C2$ (7.5) are the coefficients of the aerosol

[This is a post-referring version, Accepted in the International Journal of Applied Earth Observation and Geoinformation]
Link to the published (open access) version: https://doi.org/10.1016/j.jag.2019.101992

resistance, G (2.5) is a gain factor, and L is the soil effect constant, according to Rouse et al. (1974) and Huete (1988). Our L for the EVI and $SAVI$ were set using a sensitivity analysis, varying the factor L from -1 to 1 with intervals of 0.01. The best L-value occurred when simulated data achieved the highest r^2 with the lowest RMSE. The L-values found were 0.07 (for PAI models) and 0.37 (for the LAI models) for equations using $SAVI$; and 1 for both PAI and LAI models for equations using EVI. The number of models evaluated can be calculated using Eq. 5, where nc is the number of parameters entered into the model. All independent data were previously tested with the Variance Inflation Factor ($VIF = 1/(1 - r^2)$) to avoid any significant multicollinearity. We considered data to be independent when VIF < 10. All processing was performed using an interpreter Python 2.7.15 with only basic modules installed (freely available at https://github.com/razeayres/correlator).

$$NDVI = \left(\frac{\rho_4 - \rho_3}{\rho_4 + \rho_3}\right) \tag{2}$$

$$SAVI = \frac{(1 + L) \times (\rho_4 - \rho_3)}{L + \rho_4 + \rho_3} \tag{3}$$

$$EVI = G \times \frac{\rho_4 - \rho_3}{\rho_4 + C1 \times \rho_3 - C2 \times \rho_1 + L} \tag{4}$$

$$f(nc) = C^{nc}_{\begin{bmatrix}\rho_1 & \rho_4 & NDVI\\ \rho_2 & \rho_5 & SAVI\\ \rho_3 & \rho_7 & EVI\end{bmatrix}+(nc-1)} \times C^{nc}_{\begin{bmatrix}x & 1/x & \ln(x)\\ \log_{10}(x) & \sqrt{x} & x^2\\ e^x & & \end{bmatrix}+(nc-1)} \times \begin{cases} 1, & nc = 1 \\ C^{(nc-1)}_{\begin{bmatrix}+ & -\\ \times & \div\end{bmatrix}+(nc-2)}, & nc \geq 2 \end{cases} \tag{5}$$

Models verification

To verify the accuracy of all models in this study, we first assessed the applicability of parametric statistics to all data with the Shapiro–Wilk (for normality) and Brown–Forsythe (for

261 homoscedasticity) tests (Zar, 1996), and then we conducted a comparison between the remotely
262 sensed data and the estimates from the field observations using the Monte Carlo cross-
263 validation technique (Xu and Liang, 2001), considering 91 different sampling sizes varying
264 from 5 to 95% of the total data at 1% intervals. Each sample was evaluated by its r^2 and
265 computed as the mean of 50 random repetitions. The methods of cross-validation are widely
266 adopted, and they were used to check whether models tend to over-adjust to the *in situ* dataset
267 distribution (Hawkins, 2004). This over-adjustment would mean that excellent results would
268 be obtained only in calibration (Shao, 1993), while during verification, the accuracy of the
269 model would drastically drop. This approach allows for a good calibration (Shao, 1993). In
270 addition, we used the models proposed by Bastiaanssen (1998) (Eq. 6), Galvíncio et al. (2013)
271 (Eq. 7), Machado (2014) (Eq. 8), and Almeida et al. (2019) (Eq. 9), and derived from MODIS
272 data (MCD15A3H/A2H) to produce independent data required for comparing with our field
273 observations and for testing our models. Except for the model developed by Bastiaanssen
274 (2018), these other models were specifically developed for the Caatinga. However, the model
275 of Bastiaanssen (1998) has been widely used to estimate LAI in this region (e.g., Bezerra et al.,
276 2014; Oliveira et al., 2015; Santos et al., 2017).
277

$$LAI = -\frac{\ln\left[{(0.69 - SAVI)}/{0.59}\right]}{0.91} \quad (6)$$

$$LAI = e^{1.426+\frac{-0.542}{NDVI}} \quad (7)$$

$$LAI = 0.102 \times e^{5.341 \times NDVI} \quad (8)$$

$$LAI = 9.555 \times EVI - 1.324 \quad (9)$$

For Eqs. 6 to 9, we used the same Landsat dataset produced for the models calibrations; for the MODIS MCD15A2H/A3H products, we used all images for the entire study period (total of 830 candidate images). These products are designed to provide data with a spatial resolution of 500 m every four days (MCD15A3H) or every eight days (MCD15A2H). They are based on a complex algorithm that uses both the daily surface reflectance values of the MODIS sensor on one or both of the Terra and Aqua satellites and the data from a radiative transfer model, which are stored in a two-dimensional lookup table (Yang et al., 2006). These reflectance data are already corrected for atmospheric interferences such as atmospheric gases and aerosols, and they are freely available through the Earth Explorer online tool of the U.S. Geological Survey (https://earthexplorer.usgs.gov/). For all products, scale corrections were performed using the Geospatial Data Abstraction Library and clear land dry forest pixels were filtered using the Quality Band (QA band, value 0).

3. Results and discussion

Six of our selected models use $NDVI$, $SAVI$ and EVI as input (Eqs. 15 to 17, and 23 to 25 in Table 2). These models exhibited r^2 values ranging from 0.77 to 0.79 for PAI and 0.78 to 0.81 for LAI, and RMSE with a minimum of 0.41 m^2 m^{-2} for PAI and 0.40 m^2 m^{-2} for LAI. The $SAVI$ models (Eqs. 15 and 23) showed RMSE values smaller than the ones found for the models that use EVI and $NDVI$. We ascribe the better accuracy with the $SAVI$ models over the other vegetation indices to the fact that SAVI takes into consideration the effects of soil background, while not showing high variability as EVI does for sparsely vegetated areas, which in turn produces infrared reflectance at low levels due to dry soil background (Lu et al., 2015). In addition, $SAVI$ better reflects the surface roughness, which affects momentum, heat, and water vapor fluxes (Bastiaanssen, 1998), and varies according to the phenological stages of the Caatinga (Teixeira et al., 2008). These models are useful because they allow easy retrieval of

the PAI or LAI from remote sensing data. For example, many $NDVI$ products, using a large variety of sensor data, are freely available, and they can be used to acquire physical information for large forest areas.

Our models presented a better performance when fitted linearly rather than in any other non-linear form (Table 2). This is the opposite of what was shown by some $NDVI$–LAI relationship models (Liu et al., 2012; Tavakoli et al., 2014). Liu et al. (2012) conducted an experiment in the Ningxia Hui Autonomous District, in Northwest China, and they found saturation of $NDVI$ at high LAI values. Tavakoli et al. (2014), in 16 plots of winter wheat (*Triticum aestivum* L., cv. Cubus) in an experimental station located in Marquardt in Germany, found the best $NDVI$–LAI relation when fitting data logarithmically. In fact, this saturation of LAI as function of $NDVI$ is commonly expressed by a logarithmic relationship. However, NDVI values tend to be poorly associated with those from ground observations in SDTFs (Guzmán et al., 2019). In our study, the vegetation indices did not exhibit saturation related to the LAI of the Caatinga vegetation, which resulted in a linear covariance as reflect in Eqs. 23–25. Magalhães et al. (2018) showed that a linear model simulates better LAI in a SDTF by arguing that $NDVI$ can only saturate in vegetation types with LAI above 5 $m^2 m^{-2}$. That supports our findings since this threshold is above the values we used to develop LAI models for the Caatinga.

In this study, absolute non-saturated simulated LAI values varied from 0 to 4.56 $m^2 m^{-2}$ (0.61 to 5.23 $m^2 m^{-2}$ for PAI values), while Bastiaanssen (1998) exhibited values from 0 to ca. 4.45 $m^2 m^{-2}$ (considering only the non-saturated values), Galvíncio et al. (2013) from 0.63 to 1.98 $m^2 m^{-2}$, Machado (2014) from 0.25 to 3.7 $m^2 m^{-2}$, and Almeida et al. (2019) from ca. 0 up to 4.26 $m^2 m^{-2}$ in average. All of these previously models do not consider the temporal variations due to the phenological stages of the Caatinga on a continuous multi-year basis, thus the range of possible simulated values is smaller when compared to our models. Bastiaanssen

(1998) derived LAI using different equations for only seven types of land use cover types (cotton, maize, soy, wheat, fruit trees, vegetables, and native forests), none of which were similar to the dry forest in our study area. The study of Galvíncio et al. (2013) was based on a comparison of data obtained using an AccuPAR analyzer with indices created from spectroradiometry from a single day of measurements. The model proposed by Machado (2014) was developed in a Caatinga area of the National Park of Catimbau using only one Landsat 5 TM image, combined with 54 field-derived LAI measurements acquired three times over 20 days using simultaneous averages of diffuse light interception at five different zenith angles using sensors with fisheye lens. Almeida et al. (2019) created LAI models using the litterfall trap method in the Caatinga, and collected data for three representative species. Although the LAI models of Almeida et al. (2019) show high correlation to their field measurements, they were not able to consider the entire growth cycle in their analysis due to limitations of the litterfall fall method such as the discrete distribution of the measurements over time, and misestimation of the foliar development because of the appearance of new leaves between assessments.

PAI / LAI

Model		r^2 [1]	RMSE [2]	ρ_c	PBIAS [2]
Eq. 10	$y = 10.1 \times \left(\rho_4 - \sqrt{\rho_3}\right) + 3.1$	0.79	0.41	0.88	0.33
Eq. 11	$y = -13.2 \times \left(\sqrt{\rho_2} - \rho_4\right) + 3.1$	0.77	0.44	0.87	1.84
Eq. 12	$y = -13.5 \times \left({\log_{10}(\rho_4)}/{\ln(\rho_3)}\right) + 6.1$	0.77	0.43	0.87	-1.84
Eq. 13	$y = -20.3 \times (\rho_3 - {\rho_4}^2) + 3$	0.77	0.43	0.87	-0.83
Eq. 14	$y = -3.2 \times \left(\ln(\rho_3) \times \sqrt{\rho_4}\right) - 1.4$	0.79	0.41	0.88	-0.22
Eq. 15 [3]	$y = 3.5 \times (e^{SAVI}) - 2.7$	0.79	0.41	0.88	1.10
Eq. 16	$y = 4.8 \times (e^{EVI}) - 3.7$	0.77	0.45	0.86	3.72
Eq. 17	$y = 5 \times (NDVI^2) + 1.3$	0.79	0.43	0.89	1.04
Eq. 18	$y = \left({\rho_4}^2/\rho_1\right) - 0.1$	0.79	0.41	0.88	-0.01

Eq. 19	$y = -9.7 \times \left(\log_{10}(\rho_3) \Big/ \left(\frac{1}{\rho_4}\right) \right) - 1.2$	0.78	0.42	0.88	-4.84
Eq. 20	$y = 11.2 \times \left(\sqrt{\rho_4} - e^{\rho_3}\right) + 8.3$	0.76	0.44	0.86	7.15
Eq. 21	$y = 12.2 \times \left(\sqrt{\rho_4} - \sqrt{\rho_2}\right) - 1.2$	0.76	0.44	0.86	-0.73
Eq. 22	$y = 19.6 \times ({\rho_4}^2 - e^{\rho_3}) + 21.4$	0.78	0.42	0.87	-3.01
Eq. 23 [3]	$y = 11 \times (SAVI^2) + 0.2$	0.81	0.40	0.89	0.04
Eq. 24	$y = 6.5 \times (EVI) - 0.4$	0.78	0.42	0.88	-5.71
Eq. 25	$y = 4.9 \times (NDVI^2) + 0.1$	0.80	0.41	0.89	4.39

[1] Significant at $p = 0.05$
[2] RMSE is in $m^2\ m^{-2}$, and PBIAS is showed as percentage.
[3] L-values in the $SAVI$ calculations were 0.07 (for the PAI) and 0.37 (for the LAI).

Table 2 - Calibration of PAI and LAI models created through an iterative process using Landsat reflectance data.

The best-performing new models that use different band combinations were Eqs. 10 to 14, and 18 to 22 (Table 2). These equations may represent other physical processes and components, such as leaf etiolation and increasing protochlorophyll, which is reported to influence the blue band of the visible spectrum (ρ_1 in Eq. 17) (Gates et al., 1965). Medeiros et al. (2019) suggested the near-infrared (NIR) band may be a good indicator of leaf radiation reflectance patterns among different species, which reflect variations in leaf size, form, and type, and even plant habit. Our models used the NIR band, and they varied only to the inclusion of the red, green, and blue bands. The amount of energy reflected or absorbed in these bands varies according to the physicochemical and biophysical properties of the target (Edwards et al., 2013). All bodies reflect or emit electromagnetic radiation at different wavelengths and in different ways, and the result is a reflectance curve or spectral signature (Schmugge et al., 2002). This set of unique interactions restricts the bands that distinguish certain characteristics of a target and allows various parameters quantification (e.g., pigment concentration and plant structure complexity) (Blackburn, 2007; Dawson et al., 1998; Schmugge et al., 2002). Usually,

vegetation reflects about half of the incident radiant flux in the NIR band (Zhao et al., 2007); therefore, this is a band very sensitive to biomass and LAI. Leaves predominantly absorb energy at the blue–red spectrum and reflect the energy in the green and NIR bands because of the interaction with chlorophyll, carotenoids, and the mesophyll itself (Gates et al., 1965). Thus, the green and NIR bands are considered bands of high reflectance (Fan et al., 2018). In comparison to the green band, the NIR has a relatively higher multiple reflectance through within-canopy layers, which reduces the canopy light extinction coefficient (Zheng and Moskal, 2009).

We consider Eqs. 10, 15, and 17 to be optimal solutions for the estimation of PAI, and Eqs. 18, 23, and 25 for the estimation of LAI in the Caatinga (Table 2). Although studies have highlighted the dubious quality of data acquired by remote sensing in the blue band because of wavelength-dependent atmospheric interference (e.g., Carter et al., 2009; Motohka et al., 2009), Eq. 18 has performed very well with $r^2 = 0.79$ and RMSE = 0.41 m^2 m^{-2}, with values comparable to Eq. 23 (which does not use the blue band) with $r^2 = 0.81$ and RMSE = 0.40 m^2 m^{-2}. The greatest contribution of Eq. 18 is its natural proximity to a 1:1 relation to *in situ* measurements (ρ_c = 0.88, PBIAS = -0.01), which provides greater ability to simulate values near to zero. Although our models require observations in the NIR band, many images have NIR sensors and, if well calibrated, they allow for LAI to be estimated based on reflectance from spectral mixture or coarse resolution compositions. These images include those captured by phenological cameras, unmanned aerial vehicles, and high-resolution monitoring satellites (e.g., QuickBird and IKONOS).

The accuracy of our best models can be visualized when plotting their estimates alongside observed PAI and LAI data (Fig. 3). Our best performance models were able to emulate the variance of LAI in our study period (Table 2). Eqs. 10, 15 and 23 are biased towards overestimation (PBIAS = 0.33, 1.10 and 0.04 respectively) and Eq. 18 presented a small

underestimation bias (PBIAS = -0.01). In general, based on our findings, models developed with independent bands of a sensor produced low-magnitude values near-optimal zero, indicating accurate model simulation, while the models created using vegetation indices exhibited moderate bias.

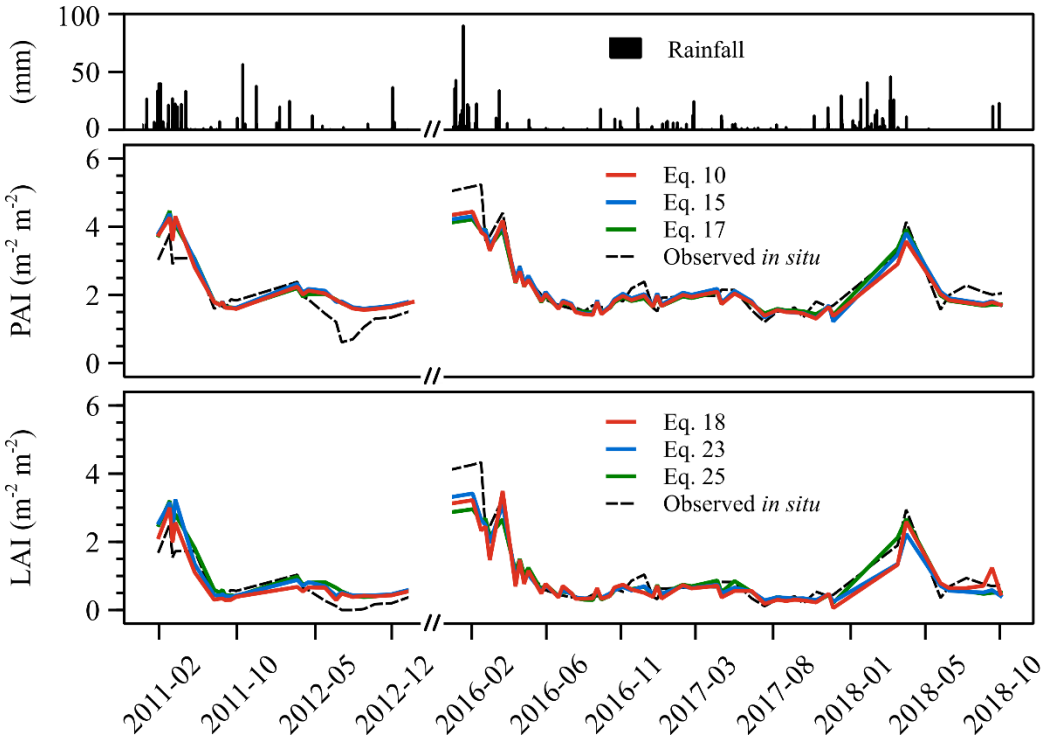

Figure 3. Comparison of temporal variation of PAI (in the middle) and LAI (bottom) observed *in situ* to the best simulated models created through an iterative process using Landsat reflectance data.

In the cross-validation analyses, Eq. 10 produced maximum values (r_{max} = 0.81) and minimum values (r_{min} = 0.68) similar to Eq. 18 (r_{max} = 0.83 and r_{min} = 0.59). In comparison, the $NDVI$, $SAVI$ and EVI models yielded higher maximum and minimum values for both PAI (r_{max} = 0.83, 0.82, and 0.80, respectively; r_{min} = 0.73 for all models) and LAI (r_{max} = 0.84, 0.85, and 0.83; r_{min} = 0.71, 0.71, and 0.69, respectively). The other models presented r values ranging from 0.64 to 0.84 (for PAI), and 0.6 to 0.83 (for LAI). The 0.01 standard deviation of

399 r was the same for all models, indicating that they are reliable. When varying the amount of
400 data taken for cross-validation from 5 to 95%, the r values tend to show minimal variations
401 (Figs. 4 and 5). However, in our verification we did not observe any statistically significant
402 pattern in correlation owing to the removal of data from the calibration of the models, which
403 confirms that these models are highly robust to estimate LAI.
404

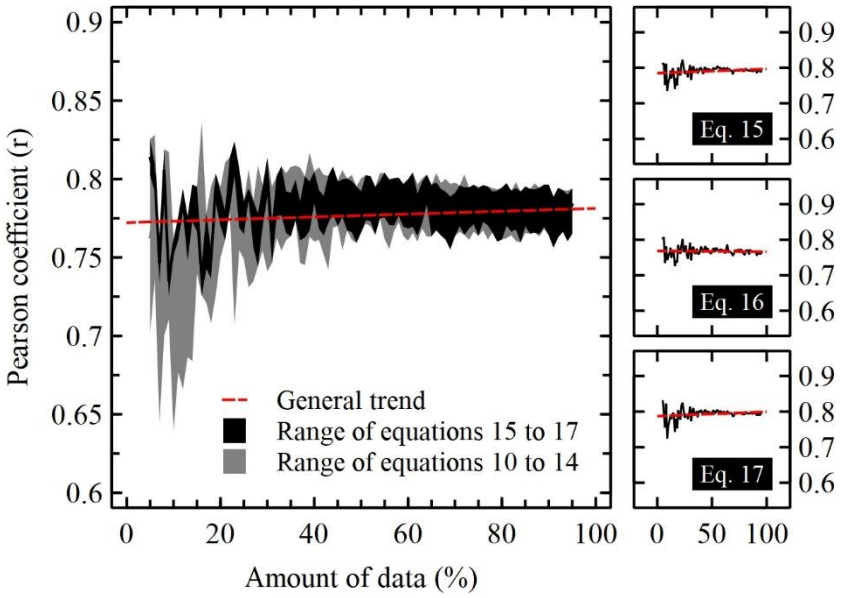

405
406 Figure 4. Cross-validation of the PAI models created through an iterative process using Landsat
407 reflectance data. Detailed validations of Eq. 15 to 17 are on the right side.
408

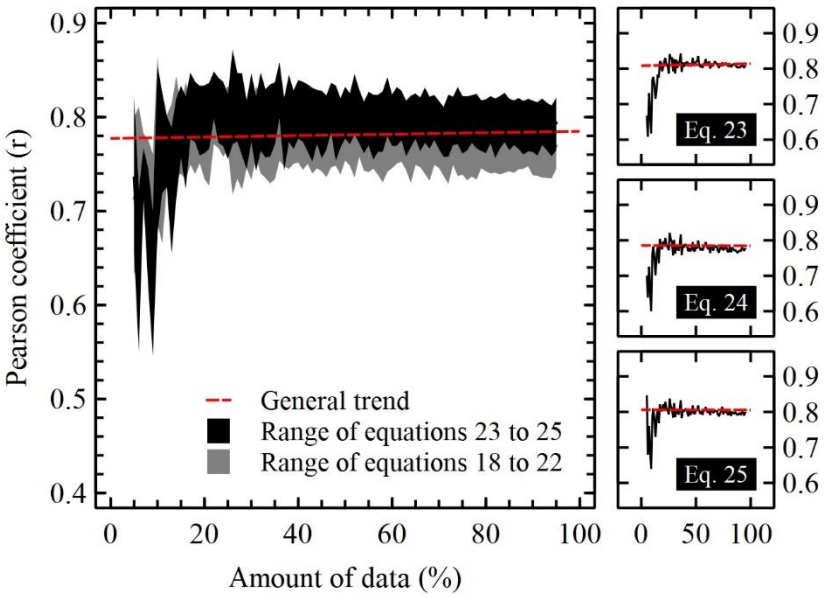

409

410 Figure 5. Cross-validation of the LAI models created through an iterative process using Landsat
411 reflectance data. Detailed cross-validations of Eqs. 23 to 25 are on the right side.

412 The approaches proposed by Bastiaanssen (1998) (Eq. 6), Galvíncio et al. (2013) (Eq.
413 7), Machado (2014) (Eq. 8), and Almeida et al. (2019) (Eq. 9), as well as the MCD15A3H/A2H
414 data underperformed compared to our models, when compared to our *in situ* PAI and LAI data
415 (Table 3), even though correlations were significant ($p < 0.05$). Eqs. 6 and 7 performed the best
416 in terms of accuracy, while Eqs. 8 and 9 presented the highest covariances. Although the
417 MODIS products are supposed to reproduce the LAI seasonality well, we observed that they
418 do not respond well for the Caatinga during the dry season; the lowest values were around 0.5
419 $m^2 m^{-2}$ when real LAI values were practically zero. We tested the fitness of MODIS products
420 against our *in situ* PAI and LAI datasets. The lower correlation with the MCD15A3H product
421 in comparison to the MCD15A2H product indicates that the proportion of high-quality data for
422 the dry forest area is lower for periods of composition of four days than for the eight-day
423 version (Table 3). These periods of composition are created from the highest value observed *in*
424 *situ*; thus, the greater the number of values available for the determination of LAI of each pixel,
425 the higher the probability of it being an accurate value. This is because data obtained by

426 satellites are influenced by a number of different atmospheric factors such as water vapor, cloud
427 cover, and aerosols, thus any given bit of satellite data may not yield accurate results (Yang et
428 al., 2006). Our results indicate that studies that rely on LAI from MODIS products for
429 vegetation assessment in SDTFs, such as the Caatinga, are likely to incorporate bias due to
430 unrealistically high LAI values during the dry season, when plants lose most of their leaves
431 and the vegetation consist predominantly of non-photosynthetic biomass (Leal et al., 2003;
432 Silva et al., 2017). The reduction of photosynthesis has direct consequences for the
433 evapotranspiration and gross primary productivity, affecting the carbon storage and CO_2
434 exchange capacity (Morais et al., 2017; Nagler et al., 2003).
435

Reference	Parameter	r^2 [1]	RMSE [2]	ρ_c	PBIAS [2]
Bastiaanssen (1998)	PAI	0.73	1.54	0.35	-69.44
	LAI	0.75	0.51	0.84	-26.53
Galvíncio et al. (2013)	PAI	0.73	1.32	0.33	-57.44
	LAI	0.72	0.52	0.75	2.33
Machado (2014)	PAI	0.76	1.28	0.61	-40.48
	LAI	0.78	1.01	0.72	43.12
Almeida et al. (2019)	PAI	0.77	1.66	0.40	-73.74
	LAI	0.77	0.65	0.81	-36.80
MCD15A3H	PAI	0.66	1.39	0.29	-60.08
	LAI	0.65	0.57	0.71	-4.00
MCD15A2H	PAI	0.77	1.26	0.38	-55.07
	LAI	0.78	0.46	0.82	8.04
Summary of selected models					
Eq. 10	PAI	0.79	0.41	0.88	0.33
Eq. 15 [3]	PAI	0.79	0.41	0.88	1.10
Eq. 17	PAI	0.79	0.41	0.89	1.04
Eq. 18	LAI	0.79	0.41	0.88	-0.01
Eq. 23 [3]	LAI	0.81	0.40	0.89	0.04
Eq. 25	LAI	0.80	0.41	0.89	4.39

[1] Significant at $p = 0.05$
[2] RMSE is in $m^2 m^{-2}$, and PBIAS is showed as percentage.
[3] *L*-values in the *SAVI* calculations were 0.07 (for the PAI) and 0.37 (for the LAI).

436 Table 3 - Comparison of the previously published models, and the MCD15A3H/A2H products
437 with *in situ* data.

The LAI in this study, as seen in all models for the Caatinga, can be defined as effective LAI, which is the portion of LAI that effectively intercepts the light, not directly considering grouped foliage. This grouping of leaves can be quantified by a vegetation dispersion parameter Ω (clumping index) (Nilson, 1971), which often can be determined by a random distribution (Chen and Black, 1992). The "true" LAI is not easy to achieve; it requires intensive fieldwork and systematic sampling, using all possible allometric relationships (Frazer et al., 1997; Weiss et al., 2004). Since the approaches of estimating PAI and LAI used in our study are based on the light extinction, the WAI values as a result of the difference between PAI and LAI are likely to be underestimated when LAI is high (Nackaerts et al., 2000; Stenberg, 1996). This is attributed to the fact that when LAI values are very high, the leaves cover the woody area and reduce the role of light interception of the branches and stems (Chen et al., 1997), which in turn leaves the PAI and LAI values very similar (e.g., Feb 2012 in Fig. 3).

Our models are easy-to-use PAI and LAI predictors that can be applied to estimate these indices for the Caatinga. The models also can be used to simulate other Caatinga types (such as in transitional areas), but since they rely on calibration coefficients, minor adjustments might be required to approximate minimum and maximum LAI. Regional applicability can be considered as moderate-high, because the phyto-physiognomy dominated by shrubs is the main and most abundant in the Caatinga (Silva et al., 2017). However, at a regional scale, our models may be used as backup models in a physical approach that does not require calibration to achieve maximum generalization. Further improvements may include (*i*) pooling coefficients adjusted for other areas of Caatinga with different levels of degradation, which could be similar to what was made by Bastiaanssen (1998) when developing LAI models; (*ii*) the adjustment of these equations using field data from other types of Caatinga vegetation, where some plants, such as Cactaceae and Bromeliaceae, may have a more significant presence, and the soil exposure may be different; (*iii*) the removal of the influence of non-photosynthetic plant

material, such as flowers, fruits and petioles, on LAI measurements; and (*iv*) approximation of LAI to more realistic values, developing and introducing a new Ω to more efficiently account for leaf dispersion directly in the models, instead of abstracting it in regression coefficients. This could solve systematic problems, such as misestimation of LAI at a given phenological stage.

4. Conclusions

Our study developed and assessed several PAI and LAI models to be realistically representative for the phenology of a typical Caatinga ecosystem. Given the high frequency of our *in situ* measurements (mostly measured on a daily or weekly basis), all Caatinga phenological stages were covered and reproduced in our models. The joint usage of ground and satellite data presented an efficient way to assess both PAI and LAI models. The results included parameterizations with the visible and infrared spectral bands, which allowed the use of many currently available datasets to estimate LAI.

The models produced results with high accuracy (up to $r^2 = 0.81$ and RMSE = 0.41 m^2 m^{-2}). The significant improvement of our models over the others used for the Caatinga is due to the consideration of WAI, which previously had not been considered in calibrations for the Caatinga, and the temporal variations of LAI, which allowed us to create more generalist models that can be used during different phenological stages of the Caatinga vegetation.

5. Acknowledgements

We thank CAPES (Brazilian Coordination for the Improvement of Higher Level Personnel) for funding this study through the project PVE A103/2013, FACEPE (*Fundação de Amparo a Ciência e Tecnologia do Estado de Pernambuco*) for funding this through the projects FACEPE APQ 0646-9.25/16 and FACEPE APQ 0062-1.07/15 (Caatinga-FLUX), and CNPq (National Council for Scientific and Technological Development of Brazil) for funding

this through the project 402834/2016-0 - CNPq Universal 01/2016. This work is also supported by the UK/Brazil Nordeste project, funded jointly through the UK Natural Environment Research Council (NE/N012526/1 ICL and NE/N012488/1 UoR) and FAPESP (The São Paulo Research Foundation) (FAPESP 2015/50488-5).

6. References

Ab'Saber, A.N., 1974. O dominio morfoclimático Semi-Árido das caatingas brasileiras. Geomorfologia 1–39.

Almeida, C.L. de, Carvalho, T.R.A. de, Araújo, J.C. de, 2019. Leaf area index of Caatinga biome and its relationship with hydrological and spectral variables. Agric. For. Meteorol. 279, 107705. https://doi.org/10.1016/j.agrformet.2019.107705

Alvares, C.A., Stape, J.L., Sentelhas, P.C., de Moraes Gonçalves, J.L., Sparovek, G., 2013. Köppen's climate classification map for Brazil. Meteorol. Zeitschrift 22, 711–728. https://doi.org/10.1127/0941-2948/2013/0507

Arnold, J.G., Srinivasan, R., Muttiah, R.S., Williams, J.R., 1998. Large-area hydrologic modeling and assessment: Part I. Model development. J. Am. Water Resour. Assoc. 34, 73–89. https://doi.org/10.1111/j.1752-1688.1998.tb05961.x

Bastiaanssen, W., 1998. Remote sensing in water resources management: the state of the art, IX. ed. International Water Management Institute (IWMI), Colombo, Sri Lanka.

Bezerra, J.M., Moura, G.B.D.A., Silva, B.B. da, Lopes, P.M.O., Silva, Ê.F. de F. e, 2014. Parâmetros biofísicos obtidos por sensoriamento remoto em região semiárida do estado do Rio Grande do Norte, Brasil. Rev. Bras. Eng. Agrícola e Ambient. 18, 73–84. https://doi.org/10.1590/S1415-43662014000100010

Bieger, K., Arnold, J.G., Rathjens, H., White, M.J., Bosch, D.D., Allen, P.M., Volk, M., Srinivasan, R., 2017. Introduction to SWAT+, a completely restructured version of the Soil and Water Assessment Tool. JAWRA J. Am. Water Resour. Assoc. 53, 115–130. https://doi.org/10.1111/1752-1688.12482

Blackburn, G.A., 2007. Hyperspectral remote sensing of plant pigments. J. Exp. Bot. 58, 855–

67. https://doi.org/10.1093/jxb/erl123

Bonan, G.B., 1995. Land-Atmosphere interactions for climate system models: coupling biophysical, biogeochemical, and ecosystem dynamical processes. Remote Sens. Environ. 51, 57–73. https://doi.org/10.1016/0034-4257(94)00065-U

Carter, G., Lucas, K., Blossom, G., Lassitter, C., Holiday, D., Mooneyhan, D., Fastring, D., Holcombe, T., Griffith, J., 2009. Remote sensing and mapping of Tamarisk along the Colorado River, USA: a comparative use of summer-acquired Hyperion, Thematic Mapper and QuickBird data. Remote Sens. 1, 318–329. https://doi.org/10.3390/rs1030318

Chen, J.M., Black, T.A., 1992. Foliage area and architecture of plant canopies from sunfleck size distributions. Agric. For. Meteorol. 60, 249–266. https://doi.org/10.1016/0168-1923(92)90040-B

Chen, J.M., Rich, P.M., Gower, S.T., Norman, J.M., Plummer, S., 1997. Leaf area index of boreal forests: Theory, techniques, and measurements. J. Geophys. Res. Atmos. 102, 29429–29443. https://doi.org/10.1029/97JD01107

Cunha, J., Nóbrega, R.L.B., Rufino, I., Erasmi, S., Galvão, C., Valente, F., 2019. Surface albedo as a proxy for land-cover clearing in seasonally dry forests: Evidence from the Brazilian Caatinga. Remote Sens. Environ. https://doi.org/10.1016/j.rse.2019.111250

Dawson, T.P., Curran, P.J., Plummer, S.E., 1998. LIBERTY—Modeling the effects of leaf biochemical concentration on reflectance spectra. Remote Sens. Environ. 65, 50–60. https://doi.org/10.1016/S0034-4257(98)00007-8

Edwards, B.L., Namikas, S.L., D'Sa, E.J., 2013. Simple infrared techniques for measuring beach surface moisture. Earth Surf. Process. Landforms 38, 192–197. https://doi.org/10.1002/esp.3319

Fan, X., Kawamura, K., Guo, W., Xuan, T.D., Lim, J., Yuba, N., Kurokawa, Y., Obitsu, T., Lv, R., Tsumiyama, Y., Yasuda, T., Wang, Z., 2018. A simple visible and near-infrared (V-NIR) camera system for monitoring the leaf area index and growth stage of Italian ryegrass. Comput. Electron. Agric. 144, 314–323. https://doi.org/10.1016/j.compag.2017.11.025

542 Fotis, A.T., Morin, T.H., Fahey, R.T., Hardiman, B.S., Bohrer, G., Curtis, P.S., 2018. Forest
543 structure in space and time: Biotic and abiotic determinants of canopy complexity and
544 their effects on net primary productivity. Agric. For. Meteorol. 250–251, 181–191.
545 https://doi.org/10.1016/j.agrformet.2017.12.251

546 Frazer, G.W., Lertzman, K.P., Trofymow, J.A., 1997. A method for estimating canopy
547 openness, effective leaf area index, and photosynthetically active photon flux density
548 using hemispherical photography and computerized image analysis techniques. Pacific
549 Forestry Centre, Victoria, B. C.

550 Galvíncio, J.D., Moura, M.S.B. de, Silva, T.G., Silva, B.B. da, Naue, C.R., 2013. LAI improved
551 to dry forest in Semiarid of the Brazil. Int. J. Remote Sens. Appl. 3, 193.
552 https://doi.org/10.14355/ijrsa.2013.0304.04

553 Gates, D.M., Keegan, H.J., Schleter, J.C., Weidner, V.R., 1965. Spectral properties of plants.
554 Appl. Opt. 4, 11. https://doi.org/10.1364/AO.4.000011

555 Guzmán, J.A., Sanchez-Azofeifa, G.A., Espírito-Santo, M.M., 2019. MODIS and PROBA-V
556 NDVI products differ when compared with observations from phenological towers at four
557 tropical dry forests in the Americas. Remote Sens. 11, 2316.
558 https://doi.org/10.3390/rs11192316

559 Hawkins, D.M., 2004. The problem of overfitting. J. Chem. Inf. Comput. Sci. 44, 1–12.
560 https://doi.org/10.1021/ci0342472

561 Huete, A.., 1988. A soil-adjusted vegetation index (SAVI). Remote Sens. Environ. 25, 295–
562 309. https://doi.org/10.1016/0034-4257(88)90106-X

563 Jacquemoud, S., Baret, F., 1990. PROSPECT: A model of leaf optical properties spectra.
564 Remote Sens. Environ. 34, 75–91. https://doi.org/10.1016/0034-4257(90)90100-Z

565 Jacquemoud, S., Verhoef, W., Baret, F., Bacour, C., Zarco-Tejada, P.J., Asner, G.P., François,
566 C., Ustin, S.L., 2009. PROSPECT+SAIL models: A review of use for vegetation
567 characterization. Remote Sens. Environ. 113, S56–S66.
568 https://doi.org/10.1016/j.rse.2008.01.026

569 Jonckheere, I., Fleck, S., Nackaerts, K., Muys, B., Coppin, P., Weiss, M., Baret, F., 2004.

570 Review of methods for in situ leaf area index determination Part I. Theories, sensors and
571 hemispherical photography. Agric. For. Meteorol. 121, 19–35.
572 https://doi.org/10.1016/j.agrformet.2003.08.027

573 Kalacska, M., Calvo-Alvarado, J.C., Sanchez-Azofeifa, G.A., 2005. Calibration and
574 assessment of seasonal changes in leaf area index of a tropical dry forest in different stages
575 of succession. Tree Physiol. 25, 733–744. https://doi.org/10.1093/treephys/25.6.733

576 Kiill, L.H.P., 2017. Caracterização da vegetação da reserva legal da Embrapa Semiárido. Doc.
577 281, Série Documentos.

578 Knote, C., Bonafe, G., Di Giuseppe, F., 2009. Leaf Area Index specification for use in
579 Mesoscale Weather Prediction Systems. Mon. Weather Rev. 137, 3535–3550.
580 https://doi.org/10.1175/2009MWR2891.1

581 Knyazikhin, Y., Martonchik, J. V., Diner, D.J. atmosphere-corrected M. data, Myneni, R.B.,
582 Verstraete, M., Pinty, B., Gobron, N., 1998. Estimation of vegetation canopy leaf area
583 index and fraction of absorbed photosynthetically active radiation from atmosphere-
584 corrected MISR data. J. Geophys. Res. Atmos. 103, 32239–32256.
585 https://doi.org/10.1029/98JD02461

586 Leal, I.R., Tabarelli, M., Silva, J.M.C., 2003. Ecologia e conservação da Caatinga. Editora
587 Universitária da UFPE, Recife.

588 Leal, I.R., Wirth, R., Tabarelli, M., 2007. Seed dispersal by ants in the semi-arid Caatinga of
589 North-East Brazil. Ann. Bot. 99, 885–94. https://doi.org/10.1093/aob/mcm017

590 Liu, F., Qin, Q., Zhan, Z., 2012. A novel dynamic stretching solution to eliminate saturation
591 effect in NDVI and its application in drought monitoring. Chinese Geogr. Sci. 22, 683–
592 694. https://doi.org/10.1007/s11769-012-0574-5

593 Lu, L., Kuenzer, C., Wang, C., Guo, H., Li, Q., 2015. Evaluation of three MODIS-derived
594 Vegetation Index time series for dryland vegetation dynamics monitoring. Remote Sens.
595 7, 7597–7614. https://doi.org/10.3390/rs70607597

596 Machado, C.C.C., 2014. Alterações na superfície do Parque Nacional do Catimbau (PE-Brasil):
597 consolidação dos aspectos biofísicos na definição dos indicadores ambientais do bioma

598 Caatinga. Universidade Federal de Pernambuco.

599 Machado, I.C.S., Barros, L.M., Sampaio, E.V.S.B., 1997. Phenology of Caatinga species at
600 Serra Talhada, PE, Northeastern Brazil. Biotropica 29, 57–68.
601 https://doi.org/10.1111/j.1744-7429.1997.tb00006.x

602 Magalhães, S.F., Calvo-Rodriguez, S., Do Espírito Santo, M.M., Sánchez Azofeifa, G.A., 2018.
603 Determining the K coefficient to leaf area index estimations in a tropical dry forest. Int. J.
604 Biometeorol. 62, 1187–1197. https://doi.org/10.1007/s00484-018-1522-6

605 Medeiros, E.S. e S., Machado, C.C.C., Galvíncio, J.D., Moura, M.S.B. de, Araujo, H.F.P. de,
606 2019. Predicting plant species richness with satellite images in the largest dry forest
607 nucleus in South America. J. Arid Environ. 166, 43–50.
608 https://doi.org/10.1016/j.jaridenv.2019.03.001

609 Menezes, R.S.C., Sampaio, E.V.S.B., Giongo, V., Pérez-Marin, A.M., 2012. Biogeochemical
610 cycling in terrestrial ecosystems of the Caatinga Biome. Brazilian J. Biol. 72, 643–53.

611 Miranda, R.D.Q., Galvíncio, J.D., Morais, Y.C.B., Moura, M.S.B. de, Jones, C.A., Srinivasan,
612 R., 2018. Dry forest deforestation dynamics in Brazil's Pontal basin. Rev. Caatinga 31,
613 385–395. https://doi.org/10.1590/1983-21252018v31n215rc

614 Morais, Y.C.B., Araújo, M. do S.B., Moura, M.S.B., Galvíncio, J.D., Miranda, R.Q., 2017.
615 Análise do sequestro de carbono em áreas de Caatinga do semiárido pernambucano. Rev.
616 Bras. Meteorol. 32, 585–599. https://doi.org/10.1590/0102-7786324007

617 Motohka, T., Nasahara, K.N., Miyata, A., Mano, M., Tsuchida, S., 2009. Evaluation of optical
618 satellite remote sensing for rice paddy phenology in monsoon Asia using a continuous in
619 situ dataset. Int. J. Remote Sens. 30, 4343–4357.
620 https://doi.org/10.1080/01431160802549369

621 Mu, Q., Heinsch, F.A., Zhao, M., Running, S.W., 2007. Development of a global
622 evapotranspiration algorithm based on MODIS and global meteorology data. Remote
623 Sens. Environ. 111, 519–536. https://doi.org/10.1016/j.rse.2007.04.015

624 Nackaerts, K., Coppin, P., Muys, B., Hermy, M., 2000. Sampling methodology for LAI
625 measurements with LAI-2000 in small forest stands. Agric. For. Meteorol. 101, 247–250.

https://doi.org/10.1016/S0168-1923(00)00090-3

Nagler, P.L., Inoue, Y., Glenn, E.., Russ, A.., Daughtry, C.S.., 2003. Cellulose absorption index (CAI) to quantify mixed soil–plant litter scenes. Remote Sens. Environ. 87, 310–325. https://doi.org/10.1016/j.rse.2003.06.001

Nilson, T., 1971. A theoretical analysis of the frequency of gaps in plant stands. Agric. Meteorol. 8, 25–38. https://doi.org/10.1016/0002-1571(71)90092-6

Norman, J.M., 1979. Modelling the complete crop canopy, in: Barfield, B.J., Gerber, J. (Eds.), Modification of the Aerial Environment. American Society of Agricultural Engineers, St. Joseph, USA, pp. 249–277.

Oliveira, L.M.M. de, Montenegro, S.M.G.L., Silva, B.B. da, Moura, A.E.S.S. de, 2015. Balanço de radiação por sensoriamento remoto em bacia hidrográfica da Zona da Mata nordestina. Rev. Bras. Meteorol. 30, 16–28. https://doi.org/10.1590/0102-778620130652

Rankine, C., Sánchez-Azofeifa, G.A., Guzmán, J.A., Espirito-Santo, M.M., Sharp, I., 2017. Comparing MODIS and near-surface vegetation indexes for monitoring tropical dry forest phenology along a successional gradient using optical phenology towers. Environ. Res. Lett. 12, 105007. https://doi.org/10.1088/1748-9326/aa838c

Rodriguez, R., Real, P., Espinosa, M., Perry, D.A., 2009. A process-based model to evaluate site quality for Eucalyptus nitens in the Bio-Bio Region of Chile. Forestry 82, 149–162. https://doi.org/10.1093/forestry/cpn045

Rouse, J.J.W., Haas, R.R.H., Schell, J.J.A.J., Deering, D.W., Harlan, J.C., 1974. Monitoring the vernal advancement and retrogradation (greenwave effect) of natural vegetation, NASA/GSFC Type III Final Report. NASA Goddard Space Flight Centre, Greenbelt, USA.

Santos, C.A.G., Silva, R.M. da, Silva, A.M., Brasil Neto, R.M., 2017. Estimation of evapotranspiration for different land covers in a Brazilian semi-arid region: A case study of the Brígida River basin, Brazil. J. South Am. Earth Sci. 74, 54–66. https://doi.org/10.1016/j.jsames.2017.01.002

Schmugge, T.J., Kustas, W.P., Ritchie, J.C., Jackson, T.J., Rango, A., 2002. Remote sensing in

654 hydrology. Adv. Water Resour. 25, 1367–1385. https://doi.org/10.1016/S0309-
655 1708(02)00065-9

656 Shao, J., 1993. Linear model selection by Cross-Validation. J. Am. Stat. Assoc. 88, 486.
657 https://doi.org/10.2307/2290328

658 Silva, G.C., Sampaio, E.V.D.S.B., 2008. Biomassas de partes aéreas em plantas da caatinga.
659 Rev. Árvore 32, 567–575. https://doi.org/10.1590/S0100-67622008000300017

660 Silva, J.M.C., Leal, I.R., Tabarelli, M., 2017. Caatinga: The largest tropical dry forest region in
661 South America. Springer International Publishing, Cham, Switzerland.
662 https://doi.org/10.1007/978-3-319-68339-3

663 Stenberg, P., 1996. Correcting LAI-2000 estimates for the clumping of needles in shoots of
664 conifers. Agric. For. Meteorol. 79, 1–8. https://doi.org/10.1016/0168-1923(95)02274-0

665 Tavakoli, H., Mohtasebi, S.S., Alimardani, R., Gebbers, R., 2014. Evaluation of different
666 sensing approaches concerning to nondestructive estimation of leaf area index (LAI) for
667 winter wheat. Int. J. Smart Sens. Intell. Syst. 7, 337–359. https://doi.org/10.21307/ijssis-
668 2017-659

669 Teixeira, A.H. de C., Bastiaanssen, W.G.M., Ahmad, M.D., Moura, M.S.B., Bos, M.G., 2008.
670 Analysis of energy fluxes and vegetation-atmosphere parameters in irrigated and natural
671 ecosystems of semi-arid Brazil. J. Hydrol. 362, 110–127.
672 https://doi.org/10.1016/j.jhydrol.2008.08.011

673 Verhoef, W., 1985. Earth observation modeling based on layer scattering matrices. Remote
674 Sens. Environ. 17, 165–178. https://doi.org/10.1016/0034-4257(85)90072-0

675 Verhoef, W., 1984. Light scattering by leaf layers with application to canopy reflectance
676 modeling: The SAIL model. Remote Sens. Environ. 16, 125–141.
677 https://doi.org/10.1016/0034-4257(84)90057-9

678 Weiss, M., Baret, F., Smith, G.J., Jonckheere, I., Coppin, P., 2004. Review of methods for in
679 situ leaf area index (LAI) determination Part II. Estimation of LAI, errors and sampling.
680 Agric. For. Meteorol. 121, 37–53. https://doi.org/10.1016/j.agrformet.2003.08.001

681 Xu, Q.-S., Liang, Y.-Z., 2001. Monte Carlo cross validation. Chemom. Intell. Lab. Syst. 56, 1–

682 11. https://doi.org/10.1016/S0169-7439(00)00122-2

683 Yang, W., Tan, B., Dong Huang, Rautiainen, M., Shabanov, N.V., Wang, Y., Privette, J.L.,
684 Huemmrich, K.F., Fensholt, R., Sandholt, I., Weiss, M., Ahl, D.E., Gower, S.T., Nemani,
685 R.R., Knyazikhin, Y., Myneni, R.B., 2006. MODIS leaf area index products: from
686 validation to algorithm improvement. IEEE Trans. Geosci. Remote Sens. 44, 1885–1898.
687 https://doi.org/10.1109/TGRS.2006.871215

688 Zar, J.H., 1996. Biostatistical Analysis, 3rd ed. Prentice Hall, Upper Saddle River.

689 Zhao, D., Huang, L., Li, J., Qi, J., 2007. A comparative analysis of broadband and narrowband
690 derived vegetation indices in predicting LAI and CCD of a cotton canopy. ISPRS J.
691 Photogramm. Remote Sens. 62, 25–33. https://doi.org/10.1016/j.isprsjprs.2007.01.003

692 Zheng, G., Moskal, L.M., 2009. Retrieving Leaf Area Index (LAI) using remote sensing:
693 theories, methods and sensors. Sensors 9, 2719–2745. https://doi.org/10.3390/s90402719
694